Homogenization and design of acoustic Willis metasurfaces

Hussein Esfahlani, Yarden Mazor, and Andrea Alù

Homogenization and Design of Acoustic Willis Metasurfaces

Hussein Esfahlani[1,2] , Yarden Mazor[3] and Andrea Alù[1,3,4]*

[1]*Photonics Initiative, Advanced Science Research Center, City University of New York, New York, NY 10031, USA*

[2]*Kymeta Corporation, Redmond, WA 98052, USA*

[3]*Department of Electrical and Computer Engineering, The University of Texas at Austin, Austin, TX 78712, USA*

[4]*Physics Program, Graduate Center of the City University of New York, New York, NY 10016, USA*

*To whom correspondence should be addressed (aalu@gc.cuny.edu)

Metasurfaces are ultrathin planar arrays of carefully tailored subwavelength particles that enable agile and flexible manipulation of the impinging waves. Originally introduced in optics, their application to acoustic waves has recently opened exciting opportunities for exotic sound control. In conventional acoustic inclusions, the interactions with the impinging pressure and velocity are decoupled, limiting the functionalities that arrays of them can achieve. While the coupling between these two quantities in symmetry-breaking inclusions, known as Willis coupling, has been discussed for several years, only recently it has been realized that these phenomena can become nonperturbative in suitably tailored resonant scatterers. Here, we explore the opportunities that these Willis meta-atoms open in the context of acoustic metasurfaces, offering new knobs to manipulate and tailor sound. The general response of Willis metasurface is analytically derived, yielding fundamental bounds and optimal surface responses enabling unprecedented control of the impinging acoustic wavefront.

1 Introduction

Acoustic metamaterials and metasurfaces have provided a rich playground for the design and engineering of acoustic waves, exhibiting unprecedented responses in the realm of wave-matter interaction [1]. An abundance of novel ideas have sprouted to achieve extreme values of material properties [2], including simultaneous negative mass density and bulk modulus [3], [4] near-zero mass density [5], [6] and compressibility [7]. In turn, these properties have enabled new functionalities, such as acoustic cloaking [8], lensing [9], non-reciprocity [10] and orbital angular momentum [11], [12]. In order to realize these concepts, significant research efforts have been also spent on the suitable homogenization [13], [14] and modeling of these structures [15].

Recently, in analogy with magneto-electric coupling in electromagnetics [11], the idea of leveraging Willis coupling, i.e., the coupling between pressure and velocity arising in asymmetric scatterers, as an additional knob to control acoustic waves has been receiving significant attention [12],[13], [16]- [17]. Homogenization techniques have been developed to describe 1D Willis metamaterials [18], and experimental measurements of Willis coupling in one-dimensional meta-atoms have been reported [19]. For a long time Willis coupling has been considered a perturbative phenomenon of limited practical relevance, however recently Willis meta-atoms with cross-coupling as large as the direct response to pressure and velocity have been proposed [20] and experimentally validated [21], and retrieval methods to measure these quantities have been developed in [22], [23]. Active acoustic and mechanical components have also been leveraged to demonstrate asymmetric Willis polarizabilities and nonreciprocal responses [24], [25]. While metasurfaces based on Willis meta-atoms have been recently considered [26]- [27], rigorous and robust modeling of the interactions among closely spaced Willis elements, which can capture their coupling and rigorously model their collective

response, is missing. Thus, a mathematical tool to understand new opportunities arising in Willis metasurfaces and the ultimate bounds in tailoring sound with such structures is required.

In this article, we establish the foundations and study the general properties of 2D arrays of Willis acoustic particles – a Willis metasurface. We rigorously model and explore the effects of inter-particle coupling in these arrays by defining an effective polarizability, which describes the array response, and evaluate the interaction coefficients within the array [28], [29]. Finally, using effective polarizability we rigorously homogenize Willis metasurfaces and model their sound interactions in an efficient way. Next, we consider the scattering of sound by a general Willis metasurface and derive transmission, reflection and absorption in terms of its effective parameters, and using these relations we derive the bounds on wave manipulation. Finally, we apply our formulation to model practical Willis metasurfaces, validating our results with full-wave simulations performed using commercial software [30].

2   Response of a single Willis particle

Consider an individual subwavelength inclusion placed in a fluid characterized by mass density ρ_0 and sound speed c_0, shown in the inset of Figure 1a. Given its small size, we can generally describe its acoustic scattering response as the superposition of an acoustic monopole and three orthogonal dipole moments induced in the particle. If the meta-atom exhibits Willis coupling, these multipole moments can be excited by both the local pressure and particle velocity, hence the general scattering process is captured by the polarizability tensor $\underline{\alpha}$ through [18], [20]

$$\begin{pmatrix} M \\ \boldsymbol{D} \end{pmatrix} = \underline{\alpha} \cdot \begin{pmatrix} p^{loc} \\ \boldsymbol{u}^{loc} \end{pmatrix} = \begin{pmatrix} \alpha^{Mp} & \boldsymbol{\alpha}^{Mu} \\ \boldsymbol{\alpha}^{Dp} & \underline{\boldsymbol{\alpha}}^{Du} \end{pmatrix} \cdot \begin{pmatrix} p^{loc} \\ \boldsymbol{u}^{loc} \end{pmatrix}, \qquad (1)$$

where $M = \int_V \rho dV$ is the acoustic monopole, $\boldsymbol{D} = \int_V \rho \boldsymbol{r} dV$ is the acoustic dipole vector, ρ is the density distribution in the particle, V is the volume of the particle, p^{loc} is the local pressure (defined as the total pressure at the center of the particle in its absence), and $\boldsymbol{u}^{loc}$ the local

velocity field. The elements of the polarizability tensor depend on the geometry, structure and material composition of the particle. In particular, α^{Mp} is a scalar that describes the monopole generated by the local pressure. Similarly, the Willis cross-coupling terms are $\boldsymbol{\alpha}^{Mu}$ (1×3 row vector), which determines the monopole excited by the local velocity, and $\boldsymbol{\alpha}^{Dp}$ (3×1 column vector), which links the local pressure to the induced dipole moment. Finally, $\underline{\boldsymbol{\alpha}}^{Du}$ (3×3 tensor) relates the induced dipole moment to the velocity field.

As an example, Figure 1b shows the geometry of an asymmetric Helmholtz resonator and Figure 1c the corresponding lossless polarizability tensor elements as a function of frequency around the resonance, derived using a numerical retrieval procedure described in [31] (based on calculating the scattered field multipole components), and an analytical model developed in detail in Appendix A – Polarizability of a Helmholtz resonator. It is observed that polarizability components derived using both methods match with high accuracy and the relevant polarizability elements go through a resonance assuming their peak values around 730 Hz.

In [20], bounds on the various elements of $\underline{\boldsymbol{\alpha}}$ for passive inclusions have been derived based on energy conservation:

$$Diag\left[k_0^3 c_0^2\left(\underline{\boldsymbol{\alpha}}^{*T}\underline{\boldsymbol{\alpha}}'\right)\right] \leq Diag\left[6\pi i\left(\underline{\boldsymbol{\alpha}}^{*T} - \underline{\boldsymbol{\alpha}}'\right)\right], \tag{2}$$

and on reciprocity:

$$\underline{\boldsymbol{\alpha}}' = \underline{\boldsymbol{\alpha}}'^{T-}, \tag{3}$$

where $\underline{\boldsymbol{\alpha}}'$ is the normalized polarizability, as defined in Appendix B – Normalized polarizability, to ensure that all terms in the matrix have the same physical units of $[m.s^2]$, and $T-$ indicates the transpose operation with sign reversal of the off-diagonal elements. The equality in (2) is satisfied for lossless particles. In the following, we will consider also particles with non-reciprocal responses, not obeying (3). While expressions (2) and (3) present two

fundamental constraints on the particle response (passivity and reciprocity), these relations can also be used as a sanity check, to verify the analytically derived or numerically calculated individual polarizability of known inclusions. For example, a hard sphere or a Helmholtz resonator like the one analyzed in Fig. 1 are both passive and reciprocal particles, thus the individual polarizabilities derived in [31] and in Appendix A – Polarizability of a Helmholtz resonator and plotted in Fig. 1 obey both (2) and (3).

Based on the symmetries of the polarizability matrix, bianisotropic particles in electromagnetics have been classified into four categories: omega, chiral, moving and Tellegen [38]. Due to the longitudinal nature of acoustic waves, however, some of the functionalities and wave-matter interactions available in electromagnetics do not find a direct acoustic analogue. We can look at the energy balance from an impinging wave [39] to introduce a basic classification of acoustic Willis inclusions. If we assume an excitation wave propagating along $\hat{z}$ and with only a $\hat{z}$ component of velocity, the extinction power from the particle can be written in closed form as

$$\Pi_{ext} = \frac{\omega|p^i|^2}{2\rho_0} Im\left[-\frac{1}{3}\alpha'^{Mp} + (\rho_0 c_0)^2 \frac{\alpha'^{Du}_{zz}}{|\eta|^2}\right] + \frac{\omega c_0 |p^i|^2}{2\sqrt{3}} Im\left(\frac{\alpha'^{Dp}_z}{\eta^*} + \frac{\alpha'^{Mu}_z}{\eta}\right), \qquad (4)$$

as derived in Appendix C – Extinction power, with $\eta = p/u$ being the wave impedance [40], which for far-field excitation is $\eta = \eta_0 = \rho_0 c_0$. The contribution of the Willis coupling term to the extracted power comes from the second expression in (4). Without loss of generality, we can write $\alpha'^{Dp}_z = \alpha'_{nR} + \alpha'_R, \alpha'^{Mu}_z = \alpha'_{nR} - \alpha'_R$, where α'_R describes the reciprocal contribution to Willis coupling, stemming from geometrical asymmetries as a time-reversal-symmetric phenomenon (satisfying relation (3)), whereas α'_{nR} captures possible nonreciprocal responses arising from a bias that breaks time-reversal symmetry, yielding an odd-symmetric response [18]. Thus, an acoustic Willis particle with $\alpha'_{nR} = 0$ is even-symmetric and $\alpha'_R = 0$ is an odd-symmetric particle. The Willis contribution to the extinction power can then be generally written as

$$\Pi_{ext,Willis} = \frac{\omega c_0 |p^i|^2}{2\sqrt{3}} Im(2\alpha'_{nR} Re[\eta^{-1}] - 2j\alpha'_R Im[\eta^{-1}]). \tag{5}$$

We can see that reciprocal particles interact with the incoming wave through their (even) Willis coefficient only with reactive (imaginary) impedances, as in a standing wave, which is analogous to *omega* particles in electromagnetics [39]. Conversely, energy extraction from traveling waves with real impedance happens through Willis coupling only when nonreciprocal (odd) interactions arise. In the case of purely odd Willis coupling, i.e., when the particle is geometrically symmetric and $\alpha'_R = 0$, the Willis particle becomes analogous to a *moving* electromagnetic particle [39].

3 Willis metasurfaces - Effective homogenized surface parameters

3.1 Effective polarizabilities

Having defined the general properties of a Willis particle, we can now extend our analysis to a Willis metasurface, consisting of a 2D square lattice of Willis inclusions with lattice constant d, shown in Figure 1a. The response of each particle is described by Eq. (1), where the local fields contain the incident field and the contribution from the other particles in the array

$$\begin{pmatrix} p^{loc} \\ u^{loc} \end{pmatrix} = \begin{pmatrix} p^i \\ u^i \end{pmatrix} + \underline{\beta} \begin{pmatrix} M \\ D \end{pmatrix} = \begin{pmatrix} p^i \\ u^i \end{pmatrix} + \begin{pmatrix} \beta^M & \beta^{pD} \\ \beta^{uM} & \underline{\beta}^D \end{pmatrix} \begin{pmatrix} M \\ D \end{pmatrix}. \tag{6}$$

The units of $\underline{\beta}$ and its blocks are the same as $\underline{\alpha}$. For normal incidence, all the excited monopoles and dipoles are equal, and symmetry considerations force $\underline{\beta}$ to be a diagonal matrix, as shown in [31] . Following (6), we hence define the effective polarizability tensor $\widehat{\underline{\alpha}}$ of the array as

$$\begin{pmatrix} M \\ D \end{pmatrix} = \widehat{\underline{\alpha}} \begin{pmatrix} p^i \\ u^i \end{pmatrix} = \begin{pmatrix} \widehat{\alpha}^{Mp} & \widehat{\underline{\alpha}}^{Mu} \\ \widehat{\alpha}^{Dp} & \widehat{\underline{\alpha}}^{Du} \end{pmatrix} \begin{pmatrix} p^i \\ u^i \end{pmatrix}. \tag{7}$$

Its expression includes the interaction coefficients and the particle polarizabilities through

$$\hat{\alpha}^{MP} = \frac{\alpha^{MP} + \alpha^{MU} \cdot \underline{\beta}^D \cdot \underline{\Delta}^{-1} \cdot \alpha^{DP}}{\Delta_M}$$

$$\hat{\boldsymbol{\alpha}}^{MU} = \frac{\boldsymbol{\alpha}^{MU} \cdot \left[\boldsymbol{I} + \underline{\boldsymbol{\beta}}^D \cdot \underline{\Delta}^{-1} \cdot \underline{\boldsymbol{\alpha}}^{DU} \right]}{\Delta_M}$$

$$\hat{\boldsymbol{\alpha}}^{DP} = \underline{\Delta}_D^{-1} \cdot \boldsymbol{\alpha}^{DP}$$

$$\hat{\underline{\boldsymbol{\alpha}}}^{DU} = \underline{\Delta}_D^{-1} \cdot \left(\beta^M (\boldsymbol{\alpha}^{DP} \otimes \boldsymbol{\alpha}^{MU}) + (1 - \alpha^{MP}\beta^M)\underline{\boldsymbol{\alpha}}^{DU} \right), \qquad (8)$$

with

$$\underline{\Delta} = \left(\boldsymbol{I} - \underline{\boldsymbol{\alpha}}^{DU} \cdot \underline{\boldsymbol{\beta}}^D \right)$$

$$\underline{\Delta}_D = \left[(1 - \alpha^{MP}\beta^M)\left(\boldsymbol{I} - \underline{\boldsymbol{\alpha}}^{DU} \cdot \underline{\boldsymbol{\beta}}^D \right) - \beta^M(\boldsymbol{\alpha}^{DP} \otimes \boldsymbol{\alpha}^{MU}) \cdot \underline{\boldsymbol{\beta}}^D \right]$$

$$\Delta_M = (1 - \alpha^{MP}\beta^M) - \beta^M \boldsymbol{\alpha}^{MU} \cdot \left(\underline{\boldsymbol{\beta}}^D \cdot \left[\underline{\Delta}^{-1} \cdot \boldsymbol{\alpha}^{DP} \right] \right), \qquad (9)$$

where $\boldsymbol{a} \otimes \boldsymbol{b}$ is the dyadic product. Several approaches can be used to efficiently evaluate the interaction coefficients, as comprehensively discussed and evaluated, for the first time to our knowledge in acoustics, in [31], and summarized in Appendix G.

3.2   Conservation of energy constraints

Following the procedure used to derive equation (2) for a single particle, we can also derive general energy conservation constraints on $\hat{\underline{\alpha}}$ for passive metasurfaces, which consequently results in constraints on $\underline{\boldsymbol{\beta}}$. We start by examining radiated (Π_{rad}) and extinction power (Π_{ext}) for a single monopole/dipole scatterer, evaluated in Appendix D - Radiated fields and power from a point source and Appendix C – Extinction power, respectively. Assuming that the scatterer is lossless, we can plug their expressions in $\Pi_{rad} = \Pi_{ext}$, yielding

$$Im\{(\alpha^{Mp})^{-1}\} = k^3 c^2/4\pi, \qquad (10)$$

for a monopole scatterer, and

$$Re\{(\alpha_{\varepsilon\varepsilon}^{Du})^{-1}\} = k^3 \omega/12\pi\rho_0 \qquad (11)$$

for a dipole scatterer, where $\varepsilon = \{x, y, z\}$. To determine the energy constraint in an array of particles, we assume a square array of tightly packed polarizable scatterers in the xy plane, for which only the zero[th] order diffraction order contributes to power considerations. In this case, we use (7), (8) and (9) to determine M and $\boldsymbol{D}$, along with the corresponding fields generated by an array of such elements as calculated explicitly in Appendix E – Fields excited by an infinite array of monopoles / dipoles, and plug these into $\Pi_{rad} = \Pi_{ext}$ [31]. This results into the compact relations

$$Im\{\beta^M\} = \frac{k^3 c^2}{4\pi} - \frac{k c^2}{2A} \tag{12}$$

$$Re\{\beta^D_{xx}\} = Re\{\beta^D_{yy}\} = \frac{k^3 \omega}{12\pi\rho_0}, Re\{\beta^D_{zz}\} = \frac{k^3 \omega}{12\pi\rho_0} - \frac{\omega^2}{2A\eta_0}. \tag{13}$$

Analogous to Eq. (2) for individual particles, conservation of energy dictates a relation on the interaction coefficients, which implies an overall bound on the effective polarizability of the metasurface. The existence of additional diffraction orders, in the case where the lattice constant d is comparable to the incidence wavelength, contributes additional terms to equation (12). These would correspond to the relative power scattered into these additional harmonics, and the balance of the total scattered power with the incident power.

3.3   Willis metasurface impedance tensors

In electromagnetics it is common to homogenize a dense metasurface that does not support higher diffraction orders using its average surface impedance tensor [28], [41]- [42]. In analogy, we can define an acoustic surface impedance that averages the induced monopole and dipole currents in the array. Following the definition of equivalent currents in Appendix F – Definition of equivalent currents, we start by defining the induced surface currents

$$\rho(u_{2z} - u_{1z}) = \frac{-i\omega M}{A} = J_M, \tag{14}$$

$$(p_2 - p_1) = -\frac{\omega^2 D}{A} = -i\omega J_D, \tag{15}$$

where A is the area of one unit cell in the array. To relate the currents to the acoustic fields, we start from Eq. (7) and define

$$\underline{\hat{\alpha}}^{-1}\begin{pmatrix} M \\ D \end{pmatrix} = \begin{pmatrix} p^i \\ u^i \end{pmatrix}, \underline{\hat{\alpha}}^{-1} = \begin{pmatrix} \hat{a}_i^{pM} & \hat{\boldsymbol{a}}_i^{pD} \\ \hat{\boldsymbol{a}}_i^{uM} & \underline{\hat{\boldsymbol{a}}}_i^{uD} \end{pmatrix}. \tag{16}$$

Using Eq. (14), (15) and (16) together with the results in Appendix E – Fields excited by an infinite array of monopoles / dipoles, and limiting ourselves for simplicity of notation to uniaxial acoustic resonators, which respond only to the $\hat{\boldsymbol{z}}$ component of velocity, we obtain

$$p_{avg} = \left(-\frac{A\hat{a}_i^{pM}}{i\omega} + \frac{c_0}{2} \right)J_M + \left(-\frac{A\hat{a}_{i,z}^{pD}}{i\omega} \right)J_D$$

$$u_{z,avg} = \left(-\frac{A\hat{a}_{i,z}^{uM}}{i\omega} \right)J_M + \left(-\frac{A\hat{a}_{i,zz}^{uD}}{i\omega} - \frac{\omega}{2i\eta_0} \right)J_D, \tag{17}$$

where it was also assumed that the monopole-velocity coupling vector $\hat{\boldsymbol{a}}_i^{uM}$ and the dipole-pressure coupling vector $\hat{\boldsymbol{a}}_i^{pD}$ have only $\hat{z}$ components, because the particles are uniaxial. This relation fully describes and captures the acoustic Willis properties of the metasurface, and extends to the acoustic domain the boundary conditions obtained in electromagnetic bianisotropic metasurfaces [28], [43]. The general expression to describe metasurfaces with arbitrary Willis inclusions using boundary impedances is outlined in [31], relating the relevant impedance expressions to the inclusion and surface properties through the polarizabilities and interaction coefficients. In addition, the metasurface is described using standard $T-$ and $\Pi-$circuit models, connecting the impedances to the reflection and transmission coefficients.

4 Reflection and transmission coefficients

Using the effective polarizabilities derived in Section 3.1, we are now ready to evaluate the reflection and transmission properties for plane wave excitation of general Willis metasurfaces.

We limit our analysis to normal incidence for simplicity of notation, but similar principles can be applied to arbitrary incidence angles [44]. Consider a plane wave incident on the array, with fields

$$p^i = p_0 e^{\pm i k_0 z} e^{-i\omega t}$$

$$\boldsymbol{u}^i = \pm \hat{z} \frac{p_0}{\eta_0} e^{\pm i k_0 z} e^{-i\omega t}, \tag{18}$$

with $\pm$ representing propagation in the $\pm \hat{z}$ direction. Using Appendix E – Fields excited by an infinite array of monopoles / dipoles, the amplitudes of reflected and transmitted fields can be written in terms of the induced monopole and dipole moments as

$$p_{ref}^{\pm} = -i \frac{\omega^{2\pm} M}{2A k_0} - \frac{\omega^{2\pm} D_z}{2A}$$

$$p_{tr}^{\pm} = p^i - i \frac{\omega^{2\pm} M}{2A k_0} + \frac{\omega^{2\pm} D_z}{2A}, \tag{19}$$

where we have again assumed that the array is dense, hence only normally outgoing waves are scattered. Next, we use the definitions of effective polarizability as in Eq. (7) to omit M and D_z and obtain the reflection and transmission coefficients as

$$R^{\pm} = \frac{i\omega^2}{2A k_0} \left(\frac{\hat{\alpha}'^{MP}}{3} \mp \frac{\hat{\alpha}_z'^{Dp} - \hat{\alpha}_z'^{Mu}}{\sqrt{3}} - \hat{\alpha}_{zz}'^{Du} \right)$$

$$T^{\pm} = 1 + \frac{i\omega^2}{2A k_0} \left(\frac{\hat{\alpha}'^{Mp}}{3} \pm \frac{\hat{\alpha}_z'^{Dp} + \hat{\alpha}_z'^{Mu}}{\sqrt{3}} + \hat{\alpha}_{zz}'^{Du} \right), \tag{20}$$

where $\hat{\alpha}'$ is the normalized effective polarizability of the array. In the reciprocal case, $\hat{\alpha}_z'^{Dp} = -\hat{\alpha}_z'^{Mu}$, the transmission is independent of Willis coupling, and therefore reciprocal Willis coefficients, which are inherently even, introduce only an asymmetry in the reflection properties, and do not control transmission. Dually, purely odd Willis coupling coefficients, associated with non-reciprocal phenomena, do not affect the reflection properties but introduce transmission asymmetries.

Using Eq. (19), the acoustic Willis metasurfaces can be modeled using a lumped circuit analogy, which provides a straightforward tool to analyze and design these structures. The derivation of the lumped circuit components in T- and Π-topologies has been explained in [31], showing that in reciprocal $(T^+ = T^-)$ and symmetric structures $(R^+ = R^-)$ the lumped circuit components follow

$$Z_1 = Z_2 = Z_0 \frac{-\omega^2 D_z^e}{[2A + \omega^2 D_z^e]}$$

$$Z_3 = Z_0 \frac{2Ak - i\omega^2 M^e + \omega^2 k D_z^e}{i\frac{\omega^2 M^e}{A}[\omega^2 D_z^e + 2A]}, \tag{21}$$

for T-topology. It is observed that for an array of reciprocal and symmetric particles, the series components are purely dipolar; however, the parallel component has the contribution of both dipole and monopole. These relations can be used to design and synthesize a Willis metasurface or retrieve the effective monopole and dipole moments of particles, when the lumped element topology of the metasurface is known.

4.1 Total reflection

Total reflection occurs in the lossless scenario when $T = 0$, which arises at the metasurface resonance. Using Eq. (20) and assuming reciprocity, the required condition to achieve fully reflective Willis metasurfaces is

$$\frac{\hat{\alpha}'^{Mp}}{3} + \hat{\alpha}_{zz}'^{Du} - \frac{2iAk_0}{\omega^2} = 0, \tag{22}$$

which corresponds to the metasurface resonance. In particular, for Eq. (22) to be satisfied we notice that the polarizability terms must be purely imaginary, or have real parts that cancel each other. Using a 2D square array of Helmholtz resonators shown in Figure 1b, whose polarizability is explicitly calculated in Appendix A – Polarizability of a Helmholtz resonator, the required particle dimensions and array configuration can be defined to support total

reflection. Figure 2(a-c) shows the absolute value of the left-hand side of Eq. (22) as we sweep one of the geometrical parameters of the resonator while the others are fixed at $a = 2cm$, $\ell = 5.6mm$, $r_{neck} = 5mm$ and $d = 5cm$. The condition for total reflection is satisfied when the magnitude goes to zero, corresponding to the dark regions in these figures. Figure 2(d-f) show the amplitude of the reflection and transmission coefficients for specific values of parameters, with values shown in each panel. The resonator dimensions can be used to control the frequency and bandwidth of the reflection response.

While Eq. (20) reveals that reciprocal Willis coupling coefficients do not play a role in the acoustic transmission through a Willis metasurface, it also discloses that the coupling terms can be used to tailor the reflection coefficient and achieve asymmetric reflection. Figure 3a shows the amplitude of the reflection and transmission coefficients for a 2D array of Helmholtz resonators for normal incident excitation. The good agreement between numerical and analytical results confirms the validity and robustness of the proposed analytical procedure to calculate the response of the Willis metasurfaces. Furthermore, the presented analytical framework can be used to gain insight into the physics of Willis particles arranged in 2D arrays. Since we are considering lossless particles, energy conservation requires that the asymmetry in reflection when excited from opposite sides is found only in terms of the phase. As an example, the phase of the reflection and transmission coefficients is shown in Figure 3b, showcasing largely different reflection phases for propagation along +z and -z.

Indeed, the phase of the reflection coefficient changes when the incident wave impinges from opposite sides, and this asymmetry can be engineered directly via the even Willis coupling coefficients. Looking closer at Eq. (19), and replacing $^{\pm}R = e^{i\varphi^{\pm}}$, $T = 0$ elucidates the relation of the reflection phase to the balance of excited monopoles and dipoles [31]

$$^{\pm}D_z^e = -\frac{A}{\omega^2}\left(1 + e^{i\varphi^{\pm}}\right), \quad ^{\pm}M^e = -i\frac{Ak}{\omega^2}\left(1 - e^{i\varphi^{\pm}}\right). \tag{23}$$

Relations derived based on effective polarizabilities, such as Eq. (20) and Eq. (22), provide a concise, accurate and design friendly model of the Willis metasurface. However, expressions that explicitly incorporate the monopole and dipole moments, such as Eq. (19) and Eq. (23), provide more physical insight on which fundamental particles contribute to a specific peculiar behavior of the metasurface.

4.2   Asymmetric absorption

Investigating the relation between reflection and transmission coefficients in Eq. (20) outlines the connection between the effective polarizability of the Willis particles and the metasurface scattering features. Reciprocity dictates that the transmission properties are equal from either direction, but by properly engineering the Willis response, we can control the reflection phase asymmetry in the lossless case, as discussed in the previous section, and more generally tailor the balance between reflection and absorption in the case in which the particles can absorb. This allows us to achieve asymmetric absorption properties with respect to the incidence direction of the acoustic waves. Figure 4 shows the reflection and transmission properties of a Willis metasurface with asymmetric reflection phase and amplitude, composed of Helmholtz resonators with similar geometrical dimensions as in the lossless case and filled with porous absorbing materials. The polarizability of the individual particles was numerically extracted from numerical simulations and then substituted into our analytical formulas to evaluate the reflection and transmission, comparing it with full-wave numerical simulations of the entire 2D array. While in the lossless case presented in Figure 3 the geometrical asymmetry responsible for Willis coupling introduces just an asymmetry in the reflection phase, in the lossy scenario it affects both amplitude and phase of the reflected fields. Good agreement between numerical and analytical results validates our model, and it captures the physics of lossy Willis metasurfaces and their potential to realize asymmetric absorption. While Eq. (20) offers the freedom to design a Willis metasurface with desired asymmetrical reflection and absorption,

the geometrical parameters of the unit cell set limit on the feasibility of the targeted amount of reflection, absorption and transmission. For example, it can be proved that the maximum amount of achievable absorption for a purely monopolar array of resonators is 50% [31], [45] and due to the highly monopolar response of the proposed Helmholtz configuration the maximum amount of absorption turns out to be $\sim 60\%$. In order to achieve total asymmetric absorption/reflection properties $\left(R^+ = 0, R^- = e^{-i\varphi}, T^{\pm} = 0\right)$, a metasurface with a specifically defined effective monopolar and dipolar behavior should be designed, which follows [31]

$$^{+}D_z^e = -\frac{A}{\omega^2}, \, ^{+}M^e = -i\frac{Ak}{\omega^2}, \, ^{-}D_z^e = \frac{A}{\omega^2}\left(1 + e^{i\varphi}\right), \, ^{-}M^e = -i\frac{Ak}{\omega^2}\left(1 - e^{i\varphi}\right) \tag{24}$$

Additional conditions and relations for Willis metasurfaces with other peculiar behaviors, such as to yield full transmission, which results in a transparent array, or total absorption, are discussed in [31]. It should be noted that the exotic responses considered here can be achieved leveraging the additional degree of freedom arising from pressure-velocity coupling, described by the Willis coefficients. This claim can become more evident when comparing the reflection and transmission coefficient of a 2D array of acoustic hard spheres, shown in Figure 12 in [31] and Willis particles in Figure 3 and Figure 4, which highlight more extreme variations, and the existence of reflection asymmetries. In general, the physical limitations stemming from reciprocity and power conservation, described in Eqs. (2) and (3), combined with the lack of additional design knobs (zero Willis coefficients), in conventional metasurfaces formed by inclusions with zero or weak Willis coupling, cannot support several of the exotic features explored in this work.

5   Conclusions

In this paper, we introduced a general analytical model to analyze and homogenize acoustic Willis metasurfaces, ideally suited for design and optimization purposes, revealing physical

insights into the effect of Willis coupling phenomena on the scattering properties of these arrays. To this end, we first rigorously calculated the interaction coefficients describing the coupling in Willis metasurfaces. Then, we employed our analytical findings to formulate an effective representation of a 2D array of bianisotropic particles in terms of both effective polarizability and homogenized metasurface impedance incorporating an effective boundary condition that utilizes monopolar and dipolar equivalent currents. Using conservation of energy, we derived the bounds of these parameters, and verified our analytical results in realistic implementations, tailored to achieve perfect reflection, asymmetric reflection and absorption, showing excellent agreement between the proposed analytical model and full-wave numerical simulations.

6 Appendices

6.1 Appendix A – Polarizability of a Helmholtz resonator

Based on the expressions given in [40], the polarizability of a spherical Helmholtz resonator shown in Figure 1(b) has been calculated in [31] materials and it is expressed as

$$\alpha^{Mp} = \frac{4\pi i}{\omega^2 k}\left[-\frac{j_0{'}(ka)}{h_0^{(1)}{'}(ka)} - \frac{ka}{3h_0^{(1)}{'}(ka)}\frac{1}{-X-iR}\right]$$

$$\alpha_z^{Mu} = \frac{4\pi}{\omega^2 k}\left[\frac{(ka)^2}{2h_0^{(1)}{'}(ka)}\frac{1}{-X-iR}\right]\frac{\omega\rho_0}{k}$$

$$\alpha_z^{Dp} = -\frac{4\pi i}{\omega^2 k^2}\left[\frac{1}{h_1^{(1)}{'}(ka)}\frac{ka}{3}\frac{sin^{\frac{3}{2}}\theta_0}{sin^{\frac{1}{2}}\theta_0}\frac{1}{-X-iR}\right]$$

$$\alpha_{zz}^{Du} = \frac{4\pi}{\omega^2 k^2}\left[3\frac{j_1{'}(ka)}{h_1^{(1)}{'}(ka)} + \frac{1}{2}\frac{(ka)^2}{h_1^{(1)}{'}(ka)}\frac{sin^{\frac{3}{2}}\theta_0}{sin^{\frac{1}{2}}\theta_0}\frac{1}{-X-iR}\right]\frac{\omega\rho_0}{k}, \tag{25}$$

where a is the radius of the resonator, $sin(\theta_0) = r_{neck}/a$, $j_m{}'$, $h_m^{(1)\prime}$ are the derivatives of the spherical Bessel and Hankel function of the 1st kind of order m, and the resonator impedance parameters are expressed as

$$R_s = \frac{\rho_0 c_0}{4\pi} k^2, C_s = \frac{4\pi a^3}{3\rho_0 c_0^2}\left(1 + \frac{1}{15}k^2 a^2\right), L_s = \frac{\rho_0}{4\pi a}(\pi - \theta_0)\cot(\theta_0/2) + L_{neck}. \quad (26)$$

The inductance correction due to the neck is $L_{neck} = \rho_0 \ell/\pi r_{neck}^2$, where ℓ is the length and r_{neck} is the radius of the neck [40]. These provide the aperture impedance

$$Z = R - iX = ka \cdot \frac{4\pi a^2}{3\rho_0 c_0}(R_s - i\omega L_s + i/\omega C_s). \quad (27)$$

6.2 Appendix B – Normalized polarizability

The normalized polarizability is defined following [20] using the relation

$$\begin{pmatrix} -\sqrt{3}M \\ ik_0 \boldsymbol{D} \end{pmatrix} = \underline{\boldsymbol{\alpha}}'\begin{pmatrix} p_{loc}/\sqrt{3} \\ \rho_0 c_0 \boldsymbol{u}_{loc} \end{pmatrix} = \begin{pmatrix} -3\alpha^{Mp} & -\frac{\sqrt{3}}{\rho_0 c_0}\boldsymbol{\alpha}^{Mu} \\ ik_0\sqrt{3}\boldsymbol{\alpha}^{Dp} & \frac{ik_0}{\rho_0 c_0}\underline{\boldsymbol{\alpha}}^{Du} \end{pmatrix}\begin{pmatrix} p_{loc}/\sqrt{3} \\ \rho_0 c_0 \boldsymbol{u}_{loc} \end{pmatrix} \quad (28)$$

6.3 Appendix C – Extinction power

Following the expressions derived in [31], the extinction power of a single particle can be written as

$$\Pi_{ext} = \frac{\omega}{2\rho_0}Im(\rho_0 c_0 \boldsymbol{u}_i^* \cdot ik_0\boldsymbol{D} - p_i^* M), \quad (29)$$

where $\boldsymbol{u}_i, p_i$ are the incident velocity and pressure fields. Using the normalized polarizability

$$\Pi_{ext} = \frac{\omega}{2\rho_0}Im\left[-\frac{1}{3}|p_i|^2\alpha^{Mp} + (\rho_0 c_0)^2 \boldsymbol{u}^{i*} \cdot \underline{\boldsymbol{\alpha}}^{Du} \cdot \boldsymbol{u}^i + \frac{\rho_0 c_0}{\sqrt{3}}(p\boldsymbol{u}^{i*} \cdot \boldsymbol{\alpha}^{Dp} - p^*\boldsymbol{u}^i \cdot \boldsymbol{\alpha}^{Mu})\right].$$

$$(30)$$

If we limit ourselves to the case of uniaxial resonators, with response in the $\hat{\mathbf{z}}$ direction, and to incident fields that propagate in the $\hat{\mathbf{z}}$ direction, we obtain

$$\Pi_{ext} = \frac{\omega}{2\rho_0} Im\left[-\frac{1}{3}|p^i|^2 \alpha'^{Mp} + (\rho_0 c_0)^2 \alpha'^{Du}_{zz}|u^i_z|^2 + \frac{\rho_0 c_0}{\sqrt{3}}\left(pu^{i*}_z \alpha'^{Dp}_z + p^* u^i_z \alpha'^{Mu}_z\right)\right]. \quad (31)$$

Since the incident wave propagates in the $\hat{\mathbf{z}}$ direction, we can write $u_z = p/\eta$ where η is the acoustic impedance of the incident fields. Substituting this into (31) yields

$$\Pi_{ext} = \frac{\omega|p^i|^2}{2\rho_0} Im\left[-\frac{1}{3}\alpha'^{Mp} + (\rho_0 c_0)^2 \frac{\alpha'^{Du}_{zz}}{|\eta|^2} + \frac{\rho_0 c_0}{\sqrt{3}}\left(\frac{\alpha'^{Dp}_z}{\eta^*} + \frac{\alpha'^{Mu}_z}{\eta}\right)\right]. \quad (32)$$

6.4 Appendix D - Radiated fields and power from a point source

6.4.1 Acoustic Monopole

If we generate sound by periodically introducing and withdrawing fluid from a small symmetric region of space, we produce a monopole. The excited pressure wave satisfies

$$\nabla^2 p - \frac{1}{c^2}\frac{\partial^2 p}{\partial t^2} = -\frac{\partial^2 M}{\partial t^2}\delta(\mathbf{r}), \quad (33)$$

where $M = \int_{V_0} \rho dV$. Using the free-space Green's function [46], we obtain the solution

$$p^M = \frac{-\omega^2 M}{4\pi r}e^{-i\omega t}e^{ikr} , \quad (34)$$

which in turn yields the total radiated power

$$\Pi^M_{rad} = \int_0^{2\pi}\int_0^{\pi}\frac{k^4 c^3|M|^2}{32\rho\pi^2 r^2}r^2 sin(\theta)d\theta d\varphi = \frac{k^4 c^3|M|^2}{8\rho\pi}. \quad (35)$$

6.4.2 Acoustic Dipole

If sound is produced by moving a portion of fluid back and forth, and no mass is added or removed, we have dipole radiation. This can also be interpreted as two equal, but anti-phase monopoles adjacent to each other. The excited pressure wave satisfies

$$\nabla^2 p - \frac{1}{c^2} \frac{\partial^2 p}{\partial t^2} = \nabla \cdot \left(\frac{\partial^2 \boldsymbol{D}}{\partial t^2} \delta(\boldsymbol{r}) \right) \tag{36}$$

where $D = \int_{V_0} \rho \boldsymbol{r} dV$. Using the free-space Green's function [46] the pressure associated with

the acoustic dipoles reads [31]

$$p = \omega^2 (\boldsymbol{D} \cdot \hat{r}) \frac{(ikr-1)}{4\pi r^2} e^{-i\omega t} e^{ikr} \tag{37}$$

and the corresponding particle velocity can be calculated as $\frac{\partial \boldsymbol{u}}{\partial t} = \frac{-1}{\rho} \nabla p$. Thus, the total radiated

power is [31]

$$\Pi_{rad}^D = \frac{k^3 \omega^3 |\boldsymbol{D}|^2}{24\rho\pi}. \tag{38}$$

6.5   Appendix E – Fields excited by an infinite array of monopoles / dipoles

6.5.1   *Infinite sheet of acoustic monopoles*

The acoustic pressure and velocity fields created by an infinite acoustic monopole sheet can be

calculated using the conservation of mass

$$\nabla \cdot \boldsymbol{u} + \frac{1}{\rho c^2} \frac{\partial p}{\partial t} = \frac{1}{\rho} \frac{\partial M}{\partial t} \delta^3(r) . \tag{39}$$

Let us use the set up shown in Figure 1(a), considering only a monopole excitation. If an

infinitesimally small volume V_0 intersects the monopole sheet, relation (39) should hold inside

V_0. Thus, using the divergence theorem we have

$$\int_{S_0} \boldsymbol{u} \cdot d\boldsymbol{s} + \frac{1}{\rho c^2} \int_{V_0} \frac{\partial p}{\partial t} dV = \frac{1}{\rho} \frac{\partial M}{\partial t} \int_{V_0} \delta^3(r) \, dV . \tag{40}$$

The radiation from an acoustic monopole is a spherically symmetric diverging wave [40], thus

the radiation field from a monopole sheet (a dense monopole array) is a plane wave. Therefore,

by substituting $p = p_0 e^{-i\omega t} e^{ikz}$ and $\boldsymbol{u} = \frac{p_0}{\eta_0} e^{-i\omega t} e^{ikz} \hat{z}$ into relation (40), and letting the

envelope approach a very flat disc around the sheet, the second integral on the left hand side

will be zero and the value of p_0 can be calculated. Thus, the pressure field radiated from an

acoustic monopole sheet reads

$$p^M = -i \frac{\omega^2 M}{2kA} e^{-i\omega t} e^{ikz}, \tag{41}$$

where A is the cross section of the integral volume and the monopole sheet and M is the total

acoustic monopole in the integral volume. The radiated power per surface area is also calculated

as

$$\Pi_{rad}^M = \oint_S \frac{1}{2} Re[p\boldsymbol{u}^*] \cdot d\boldsymbol{s} = \frac{\omega^4 |M|^2}{4\eta_0 A k^2}. \tag{42}$$

6.5.2   Infinite sheet of acoustic in-plane dipoles

Using the definition of acoustic dipole, the problem of radiation from an acoustic sheet of in-

plane dipoles can be interpreted as the superposition of two out of phase monopole sheets

shifted in the x or y direction by δ, where $\delta \rightarrow 0$. Hence, using (41) and considering that the

radiation of the monopole sheet is not a function of x or y, we can write for in-plane acoustic

dipoles D_x and D_y

$$p^{D_x} = p^{D_y} = \lim_{\delta \to 0} \left\{ p^M_{-\frac{\delta}{2}} - p^M_{+\frac{\delta}{2}} \right\} = 0. \tag{43}$$

Using relation (43) we conclude that the radiated power per surface area is also zero

$$\Pi_{rad}^{D_x} = \Pi_{rad}^{D_y} = 0. \tag{44}$$

6.5.3   Infinite sheet of acoustic out-of-plane dipoles

The acoustic pressure and velocity fields created by an infinite sheet of acoustic out of plane

dipoles can be calculated using conservation of momentum

$$\nabla p + \rho \frac{\partial \boldsymbol{u}}{\partial t} = \frac{\partial^2 D_z}{\partial t^2} \delta^3(r)\hat{z}. \tag{45}$$

If an infinitesimally small volume V_0 intersects the dipole sheet, the relation (45) should hold inside V_0. Thus, using the divergence theorem we have

$$\int_{S_0} p d\boldsymbol{s} + \rho \int_{V_0} \frac{\partial \boldsymbol{u}}{\partial t} dV = \frac{\partial^2 D_z \hat{z}}{\partial t^2} \int_{V_0} \delta^3(r) \, dV. \tag{46}$$

From similar considerations, we assume that the radiation from a tightly arranged dipole array is a plane wave, and utilize the same mathematical process, to obtain

$$p_{\pm}^{D_z} = \mp \frac{\omega^2 D_z}{2A} e^{-i\omega t} e^{\pm ikz}, \tag{47}$$

and

$$\Pi_{rad}^{D_z} = \oint_S \frac{1}{2} Re[p\boldsymbol{u}^*] \cdot d\boldsymbol{s} = \frac{\omega^4 |D_z|^2}{4\eta A}, \tag{48}$$

where p_+ and p_- are the propagating pressure field in the front $(+\hat{z})$ and back $(-\hat{z})$ of the dipole sheet, respectively.

6.6   Appendix F – Definition of equivalent currents

Let us consider a 2D square lattice populated by acoustic monopoles M and acoustic dipoles D_z, with $\hat{z}$ being the normal to the array plane. If we start from the mass conservation

$$\nabla \cdot \boldsymbol{u} + \frac{1}{\rho c_0^2} \frac{\partial p}{\partial t} = q, \tag{49}$$

where q is a source term associated with time variation of mass in space – typical of monopoles, and employ a localization process by volume integrating the equation inside a very thin box containing the surface, we find that

$$\rho(u_{2z} - u_{1z}) = \frac{-i\omega M}{A}, \tag{50}$$

where M is the acoustic monopole defined by Eq. (1). Thus, we can define an equivalent monopole current $J_M = -i\omega M/A$ and we obtain the familiar form of boundary condition

$$\rho(u_{2z} - u_{1z}) = J_M.\tag{51}$$

Alternatively, we start from the conservation of momentum

$$\nabla p + \rho \frac{\partial \boldsymbol{u}}{\partial t} = f,\tag{52}$$

f being a source term associated with the force per unit volume exerted on the fluid – typical of dipoles. If we follow the same procedure, we obtain

$$(p_2 - p_1) = -\frac{\omega^2 D}{A}.\tag{53}$$

If we define $J_D = -i\omega D/A$, then we obtain the boundary condition as

$$(p_2 - p_1) = -i\omega J_D.\tag{54}$$

6.7 Appendix G – Interaction coefficients

The closed form relations for pressure and velocity interaction coefficients have been developed using three different methods and explained in the [31], which is presented here:

$$\beta^M = \frac{-\omega^2}{2\pi h}\left\{i\pi\left(\frac{1}{kd} - \frac{1}{2}\right) + \left(\gamma + ln\frac{kd}{4\pi}\right) + 2\pi\sum_{l=1}^{\infty}\left(\frac{1}{\sqrt{(2l\pi)^2 - (kd)^2}} - \right.\right.$$

$$\left.\left.\frac{1}{2l\pi}\right) + 4\sum_{n=1}^{\infty}\sum_{m=1}^{\infty}K_0\left(n\left(\frac{d}{h}\right)\sqrt{(2\pi m)^2 - (kh)^2}\right) - ln\left[2\,sin\left(\frac{kh}{2}\right)\right] + i\frac{(\pi-kh)}{2}\right\}\tag{55}$$

$$\beta_{xx}^D = \frac{kc}{\rho}\left\{\sum_{n=1}^{\infty}\sum_{m=1}^{\infty}\frac{8i\pi m^2}{h^3}K_0\left(\frac{nd}{h}\sqrt{(2\pi m)^2 - (kh)^2}\right) - \frac{ik^2}{2\pi h}ln\left(2\,sin\left(\frac{kh}{2}\right)\right) - \frac{k^2}{4\pi h}(\pi - \right.$$

$$\left. kh) - \frac{ik}{\pi h^2}Cl_2(kh) - \frac{i}{\pi h^3}Cl_3(kh) + \frac{k^2}{4h} - \frac{k^3}{6\pi}\right\}\tag{56}$$

$$\beta_{yy}^D = \frac{kc}{\rho}\left\{\sum_{m=1}^{\infty}\sum_{n=1}^{\infty}\frac{8i\pi n^2}{d^3}K_0\left(\frac{mh}{d}\sqrt{(2\pi n)^2 - (kd)^2}\right) - \frac{ik^2}{2\pi d}ln\left(2\,sin\left(\frac{kd}{2}\right)\right) - \frac{k^2}{4\pi d}(\pi - \right.$$

$$\left. kd) - \frac{ik}{\pi d^2}Cl_2(kd) - \frac{i}{\pi d^3}Cl_3(kd) + \frac{k^2}{4d} - \frac{k^3}{6\pi}\right\}\tag{57}$$

$$\beta_{zz}^D = \frac{k^2 c}{2\pi h^2 \rho} \left\{ \sum_{n=1}^{\infty} -\frac{\pi kh}{2} \left[H_0^{(1)}(nkd) + H_2^{(1)}(nkd) \right] + \frac{2i}{kh} \sum_{m=1}^{\infty} [(2\pi m)^2 - \right.$$

$$(kh)^2] \left[K_2 \left(\frac{nd}{h} \sqrt{(2\pi m)^2 - (kh)^2} \right) - K_0 \left(\frac{nd}{h} \sqrt{(2\pi m)^2 - (kh)^2} \right) \right] - \frac{\pi kh}{4} + \frac{(kh)^2}{6} + iCl_2(kh) +$$

$$\left. \frac{i}{kh} Cl_3(kh) \right\} \tag{58}$$

Where k is the wave number in the medium and h and d, are the periodicity of the array in $\hat{x}$ and $\hat{y}$, respectively. It should be noted that the interaction coefficient forms a diagonal matrix and all the non-diagonal terms are zero.

7 References

[1] S. A. Cummer, J. Christensen and A. Alù, "Controlling sound with acoustic metamaterials," *Nat. Rev. Mater,* vol. 1, no. 3, p. 16001, 2016.

[2] Z. Liang and J. Li, "Extreme acoustic metamaterial by coiling up space," *Physical Review Letters,* vol. 108, no. 114301, 2012.

[3] H. Esfahlani, S. Karkar, H. Lissek and J. R. Mosig, "Acoustic dispersive prism," *Sci. Rep.,* vol. 6, p. 18911, 2016.

[4] H. Esfahlani, S. Karkar, H. Lissek and J. R. Mosig, "Exploiting the leaky-wave properties of transmission-line metamaterials for single-microphone direction finding," *J. Acoust. Soc. Am.,* vol. 139, no. 6, p. 3259–3266, 2016.

[5] R. Fleury and A. Alu, "Extraordinary sound transmission through density-near-zero ultranarrow channels," *Physical review letters,* vol. 111, no. 5, 2013.

[6] Y. Jing, J. Xu and N. X. Fang, "Numerical study of a near-zero-index acoustic metamaterial," *Physics Letters A,* vol. 376, p. 2834–2837, 2012.

[7] N. Cselyuszka, M. Sečujski and V. C. Bengin, "Compressibility-near-zero acoustic metamaterial," *Physics Letters A,* vol. 378, p. 1153–1156, 2014.

[8] S. Zhang, C. Xia and N. Fang, "Broadband acoustic cloak for ultrasound waves," *Phys. Rev. Lett.,* vol. 106, no. 2, p. 024301, 2011.

[9] L. Zigoneanu, B. I. Popa and S. A. Cummer, "Design and measurements of a broadband two-dimensional acoustic lens," *Phys. Rev. B - Condens. Matter Mater. Phys.,* vol. 84, no. 2, p. 024305, 2011.

[10] R. Fleury, D. L. Sounas, C. F. Sieck, M. R. Haberman and A. Alù, "Sound isolation and giant linear nonreciprocity in a compact acoustic circulator," *Science,* vol. 343, no. 6170, p. 516–519, 2014.

[11] H. Esfahlani, H. Lissek and J. R. Mosig, "Generation of acoustic helical wavefronts using metasurfaces," *Phys. Rev. B,* vol. 95, no. 2, p. 024312, 2017.

[12] S.-W. Fan, Y.-F. Wang, L. Cao, Y. Zhu, A.-L. Chen, B. Vincent, B. Assouar and Y.-S. Wang, "Acoustic vortices with high-order orbital angular momentum by a continuously tunable metasurface," *Applied Physics Letters,* vol. 116, no. 16, 2020.

[13] A. N. Norris, A. L. Shuvalov and A. A. Kutsenko, "Analytical formulation of three-dimensional dynamic homogenization for periodic elastic systems," *in Proceedings of the Royal Society A: Mathematical, Physical and Engineering Science,* vol. 468, 2012.

[14] M. Yang, G. Ma, Y. Wu, Z. Yang and P. Sheng, " Homogenization scheme for acoustic metamaterials," *Phys. Rev. B - Condens. Matter Mater. Phys.,* vol. 89, no. 6, p. 064309, 2014.

[15] F. Bongard, H. Lissek and J. R. Mosig, "Acoustic transmission line metamaterial with negative/zero/positive refractive index," *Phys. Rev. B - Condens. Matter Mater. Phys.,* vol. 82, no. 9, p. 094306, 2010.

[16] J. R. Willis, "Dynamics of Composites," *in Continuum Micromechanics,* p. 265–290., 2013.

[17] R. Pernas-Salomón and S. Gal, "Fundamental principles for generalized Willis metamaterials," *Physical Review Applied ,* vol. 14, no. 6 , p. 064005, 2020.

[18] C. F. Sieck, A. Alù and M. R. Haberman, "Origins of Willis coupling and acoustic bianisotropy in acoustic metamaterials through source-driven homogenization," *Phys. Rev. B,* vol. 96, no. 10, p. 104303, 2017.

[19] M. B. Muhlestein, C. F. Sieck, P. S. Wilson and M. R. Haberman, "Experimental evidence of Willis coupling in a one-dimensional effective material element," *Nat. Commun.,* vol. 8, p. 15625, 2017.

[20] L. Quan, Y. Ra'Di, D. L. Sounas and A. Alù, "Maximum Willis Coupling in Acoustic Scatterers," *Phys. Rev. Lett.,* vol. 120, no. 25, p. 254301, 2018.

[21] A. Melnikov, Y. K. Chiang, L. Quan, S. Oberst, A. Alù, S. Marburg and D. Powell, "Acoustic meta-atom with experimentally verified maximum Willis coupling," *Nature communications,* vol. 10, no. 1, pp. 1-7, 2019.

[22] X. Su and A. N. Norris, "Retrieval method for the bianisotropic polarizability tensor of Willis acoustic scatterers," *Phys. Rev. B,* vol. 98, no. 17, p. 174305, 2018.

[23] J. Jordaan, S. Punzet, A. Melnikov, A. Sanches, S. Oberst, S. Marburg and D. Powell, "Measuring monopole and dipole polarizability of acoustic meta-atoms," *Appl. Phys. Lett.,* vol. 113, no. 22, p. 224102, 2018.

[24] Y. Zhai, H.-S. Kwon and B.-I. Popa, "Active Willis metamaterials for ultracompact nonreciprocal linear acoustic devices," *Physical Review B ,* vol. 99, no. 22, p. 220301, 2019.

[25] Y. Chen, X. Li, G. Hu, M. R. Haberman and G. Huang, "An active mechanical Willis meta-layer with asymmetric polarizabilities," *Nature communications,* vol. 11, no. 1, pp. 1-8, 2020.

[26] B. I. Popa, Y. Zhai and H. S. Kwon, "Broadband sound barriers with bianisotropic metasurfaces," *Nat. Commun.,* vol. 9, no. 1, 2018.

[27] J. Li, C. Shen, A. Díaz-Rubio, S. A. Tretyakov and S. A. Cummer, "Systematic design and experimental demonstration of bianisotropic metasurfaces for scattering-free manipulation of acoustic wavefronts," *Nat. Commun.,* vol. 9, no. 1, 2018.

[28] S. Tretyakov, Analytical modeling in applied electromagnetics, Artech House, 2003.

[29] V. V. Yatsenko, S. I. Maslovski, S. A. Tretyakov, S. L. Prosvirnin and S. Zouhdi, " Plane-wave reflection from double arrays of small magnetoelectric scatterers," *IEEE Trans. Antennas Propag.,* vol. 51, no. 1, pp. 2-11, 2003.

[30] "www.comsol.com," Multiphysics, COMSOL. [Online].

[31] *Supporting material.* See also [32]-[37] therein.

[32] D. Pozar, Microwave engineering, John wiley & sons, 2011.

[33] R. A. Shore and A. D. Yaghjian, "Traveling waves on two- and three-dimensional periodic arrays of lossless scatterers," *Radio Sci,* vol. 42, no. 6, 2007.

[34] J. A. Stratton, Electromagnetic theory, New York: McGraw-Hill Book Company, 1941.

[35] I. M. Gradshtein and I. S. Ryzhik, Table of integrals, series, and products, Academic press, 2014.

[36] E. Skudrzyk, Foundations of acoustics : basic mathematics and basic acoustics, Springer, 2013.

[37] E. M. Viggen, " Acoustic multipole sources from the Boltzmann equation," *arXiv preprint arXiv:1302.3764,* 2013.

[38] Y. Ra'di, C. R. Simovski and S. A. Tretyakov, "Thin Perfect Absorbers for Electromagnetic Waves: Theory, Design, and Realizations," *Phys. Rev. Appl.,* vol. 3, no. 3, p. 037001, 2015.

[39] Y. Ra'Di and S. A. Tretyakov, "Balanced and optimal bianisotropic particles: Maximizing power extracted from electromagnetic fields," *New J. Phys.,* vol. 15, p. 053008, 2013.

[40] P. M. Morse and K. U. Ingard, Theoretical acoustics, New York: McGraw-Hill, 1968.

[41] M. Albooyeh, S. Tretyakov and C. Simovski, "Electromagnetic characterization of bianisotropic metasurfaces on refractive substrates: General theoretical framework," *Ann. Phys.,* vol. 528, no. 9-10, p. 721–737, 2016.

[42] A. Epstein and G. V. Eleftheriades, "Arbitrary power-conserving field transformations with passive lossless omega-type bianisotropic metasurfaces," *IEEE Trans. Antennas Propag.,* vol. 64, no. 9, p. 3880–3895, 2016.

[43] C. L. Holloway, D. C. Love, E. F. Kuester, J. A. Gordon and D. A. Hill, "Use of generalized sheet transition conditions to model guided waves on metasurfaces/metafilms," *IEEE Trans. Antennas Propag.,* vol. 60, no. 11, p. 5173–5186, 2012.

[44] M. Yazdi and M. Albooyeh, "Analysis of metasurfaces at oblique incidence," *IEEE Transactions on Antennas and Propagation,* vol. 65, no. 5, pp. 2397-2404, 2017.

[45] A. D. Lapin, "Monopole-dipole type resonator in a narrow pipe," *Acoust. Phys.,* vol. 49, no. 6, p. 731–732, 2003.

[46] L. E. Kinsler, Fundamentals of acoustics, New York: John Wiley & Sons, 2000.

[47] G. W. Milton and J. R. Willis, "On modifications of Newton's second law and linear continuum elastodynamics," *Proc. R. Soc. A Math. Phys. Eng. Sci.,* vol. 463, no. 2079, p. 855–880, 2007.

[48] G. W. Milton, M. Briane and J. R. Willis, "On cloaking for elasticity and physical equations with a transformation invariant form," *New J. Phys.,* vol. 8, no. 246, 2006.

[49] H. J. Bilow, "Guided Waves on a Planar Tensor Impedance Surface," *IEEE Trans. Antennas Propag.,* vol. 51, no. 10 II, p. 2788–2792, 2003.

[50] K. Achouri, M. A. Salem and C. Caloz, "General Metasurface Synthesis Based on Susceptibility Tensors," *IEEE Trans. Antennas Propag.,* vol. 63, no. 7, p. 2977–2991, 2015.

[51] L. Quan, D. L. Sounas and A. Alù, "Nonreciprocal Willis coupling in zero-index moving media," *Phys. Rev. Lett.,* vol. 123, no. 064301, 2019.
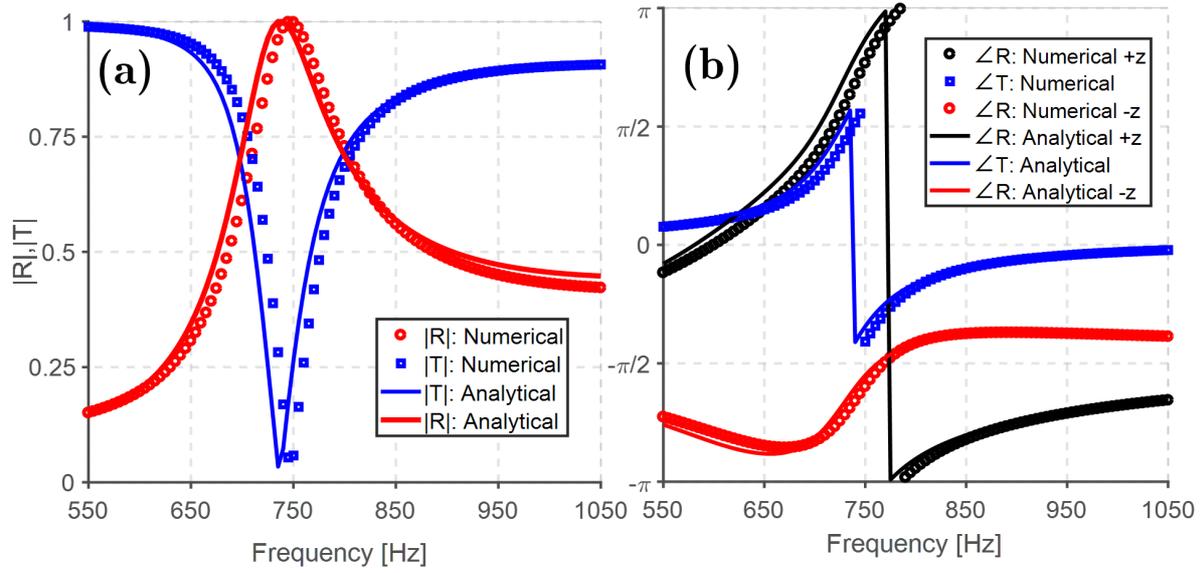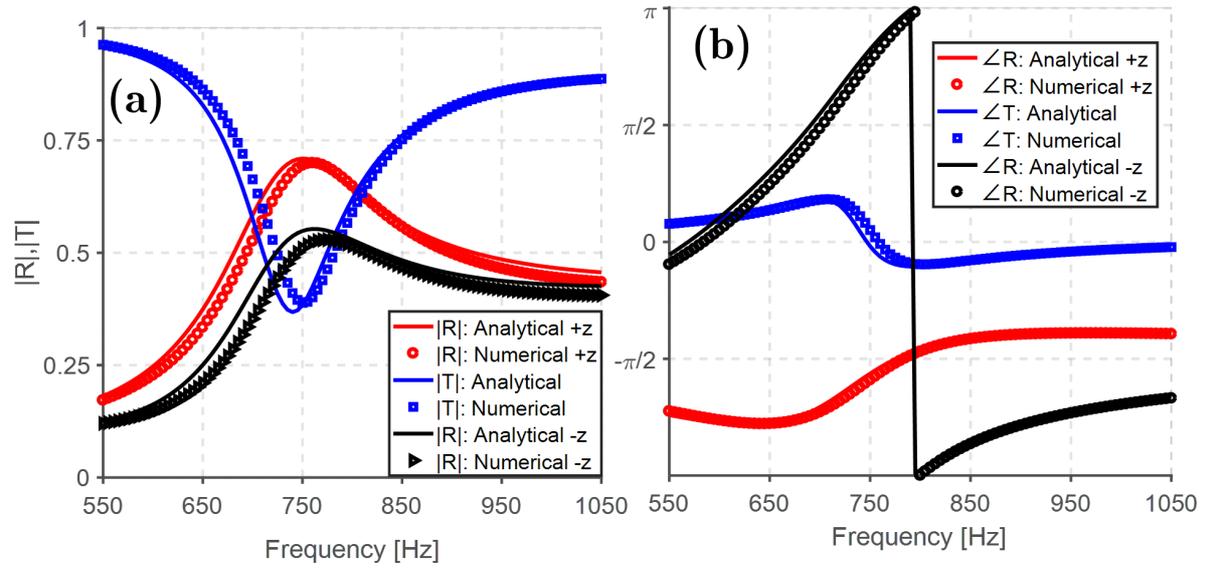
Figures
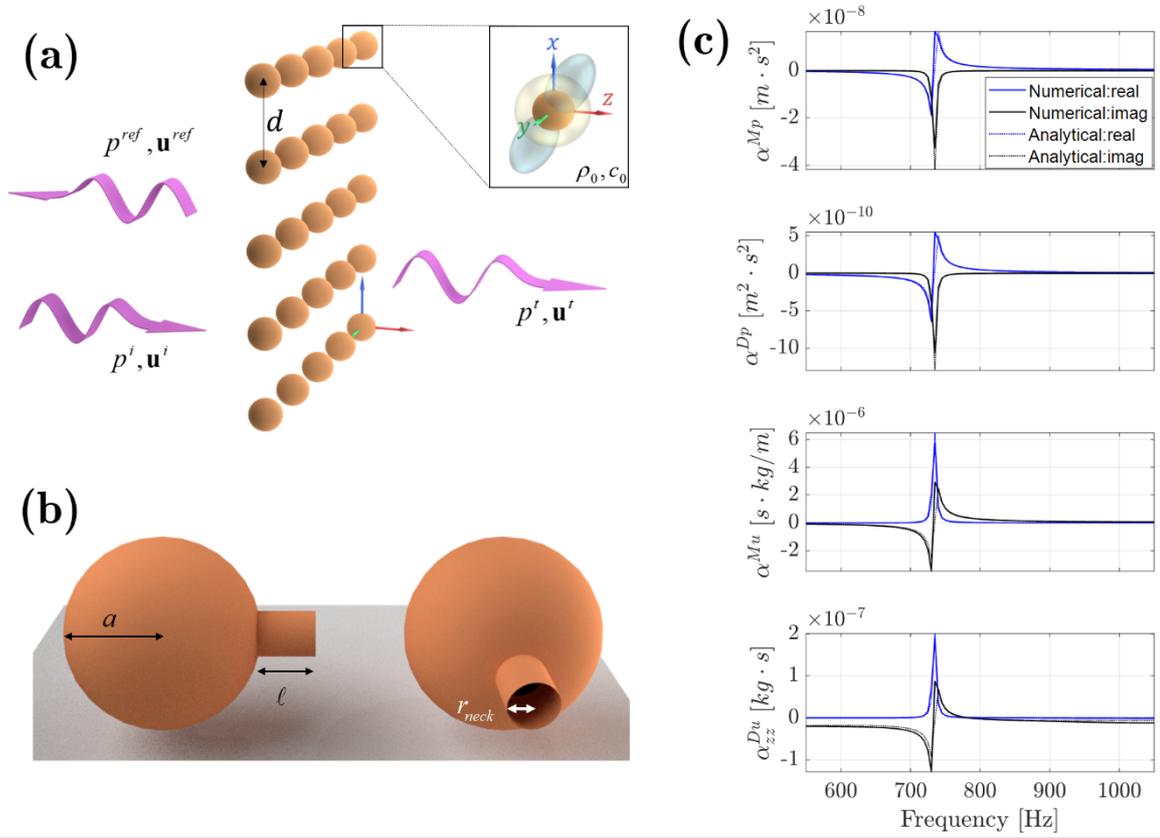
Figure 1. (a) An acoustic Willis metasurface composed of an infinite array of Willis particles (one shown in the inset) in a square lattice. In response to an incident plane wave, the array scatters reflected and transmitted plane waves driven by the induced monopole and dipole moments, with patterns depicted by yellow and green shapes in the inset. (b) Geometry of a Helmholtz resonator. (c) Acoustic polarizability of the lossless Helmholtz resonator retrieved numerically and compared to our analytical model. In this example $r_{neck} = 5mm$, $a = 20mm$, $\ell = 5.6mm$.
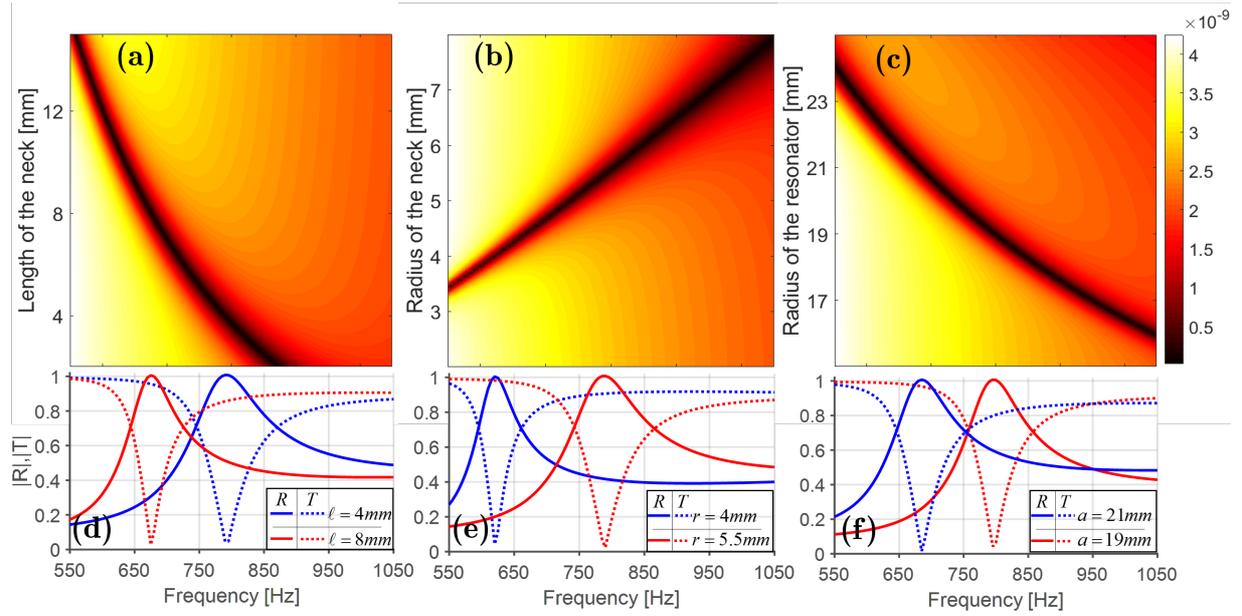
Figure 2. Absolute value of the left-hand side in Eq. (22). The zeros (corresponding to dark curves) imply a full reflective Willis metasurface. The surface consists of a square lattice of Helmholtz resonators with base dimensions $a = 2[cm]$, $\ell = 5.6[mm]$, $r_{neck} = 5[mm]$ and lattice constant $d = 5[cm]$. For each plot, three of the parameters are fixed and Eq. (22) is swept over (a) length of the neck ℓ, (b) radius of the neck r_{neck} and (c) radius of the resonator a. (d) A cross section of the reflection and transmission coefficient for two different neck lengths. (e),(f) same as (d), but for the neck radius and resonator radius, respectively.

Figure 3. Analytically vs numerically calculated reflection and transmission coefficients of a 2D array of lossless spherical Helmholtz resonators excited by a normally incident wave. (a) Amplitude, (b) phase. The geometrical parameters are $a = 2[cm]$, $\ell = 5.6[mm]$, $r_{neck} = 5[mm]$ and lattice constant $d = 5[cm]$.

Figure 4. Analytical vs numerical reflection and transmission coefficients of a 2D array of lossy spherical Helmholtz resonator subject to normal incident wave (a) Amplitude (b) Phase. Helmholtz resonator and array dimensions are the same as Figure 3, while the inner part of the resonator has been filled with a porous material of thickness $t_l = 3[mm]$ and flow resistivity $R_f = 1573.4[kg/(m^3s)]$.